Macromolecules

Article

pubs.acs.org/Macromolecules

Nanostructure Evolution during Relaxation from a Large Step Strain in a Supramolecular Copolymer-Based Hydrogel: A SANS Investigation

Clinton G. Wiener,[†] Chao Wang,[†] Yun Liu,[‡] R. A. Weiss,*[,†] and Bryan D. Vogt*[,†]

[†]Department of Polymer Engineering, University of Akron, Akron, Ohio 44325, United States

[‡]Center for Neutron Research, National Institute of Standards and Technology, Gaithersburg, Maryland 20899, United States

Supporting Information

ABSTRACT: The nanostructure changes associated with stress dissipation in a tough, supramolecular hydrogel were determined by small-angle neutron scattering (SANS) and compared with stress-relaxation measurements to understand the molecular origin of the toughness. The hydrogels were formed from random copolymers of *N*,*N*-dimethylacrylamide (DMA) and 2-(*N*-ethylperfluorooctane sulfonamido)ethyl acrylate (FOSA), which exhibit a microphase-separated morphology with physical cross-links formed by the FOSA nanodomains connected by DMA chains. The stress relaxation behavior following a step strain was fit using seven exponentials with relaxation times that spanned 5 orders of magnitude. The deformation and relaxation of the FOSA nanodomains and network chains were independently resolved using two different contrasts with SANS experiments. Stretching of the hydrogel produced anisotropic scattering at both contrasts examined. The DMA network chains relaxed to an isotropic state at a fast rate that corresponded to the shorter stress relaxation time, while the nanodomain structure relaxed slower and did not fully relax after 7 h. These SANS measurements provide correlations between relaxations at the macroscopic (stress) and microscopic (network chains and nanodomains) scales.

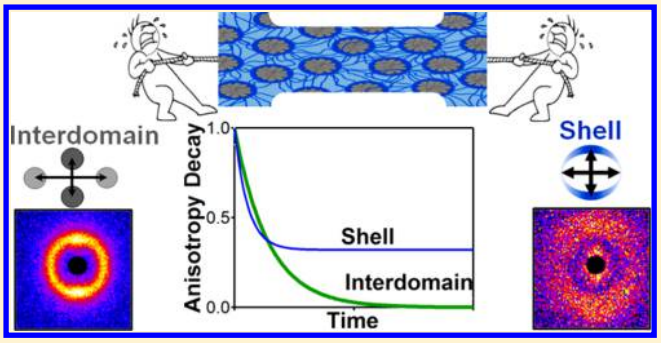

INTRODUCTION

Rapid developments over the past decade have enabled the fabrication of hydrogels that are highly swollen, tough, and ductile through a variety of methods.[1−5] Those methods tend to incorporate a network that provides a stress relief mechanism to dissipate energy on loading and prevent catastrophic failure.[2] For double network hydrogels, the rupture of a sacrificial network[6] provides toughness, and these permanent changes to the network can be assessed using tensile hysteresis and equilibrium swelling.[7] Small-angle neutron scattering (SANS) was able to provide molecular insights into the structure and origins of toughness of these double network hydrogels.[7,8] Alternatively, the incorporation of transient, reversible physical bonds, such as hydrophobic associations,[9] hydrogen bonds,[10] or ionic bonds,[11] provides a simple route to provide energy dissipation. Physical bonds can rearrange to relieve stress but then re-form to restore the network.[9] However, there is little direct knowledge about how these physical bonds rearrange to dissipate energy and provide high toughness to hydrogels. In order to indirectly examine the deformation of a network, nanoparticle tracers have been added to hydrogels,[12] and that work found that the networks deformed in either an affine or a nonaffine manner depending on the network connectivity and homogeneity. That technique, however, has issues with systems that can relieve stress by relaxation and network rearrangements, which are common attributes in tough hydrogels.

We have previously shown that the hydrophobic aggregates (nanodomains) that comprise the cross-links in a hydrogel based on a random copolymer of 2-(*N*-ethylperfluorooctane sulfonamido)ethyl acrylate (FOSA) and *N*,*N*-dimethylacrylamide (DMA) can be characterized by small angle x-ray scattering (SAXS) and SANS.[13,14] Contrast matching using H_2O/D_2O in these DMA/FOSA hydrogels to isolate the scattering of the FOSA aggregates and the DMA chains has shown that the nanostructure consists of a relatively narrow distribution of spherical glassy FOSA nanodomains[15] that are surrounded by a layer of water-depleted DMA.[14] The ability to isolate the effective cross-links, i.e., the nanodomains in that system, provides a route to directly elucidate how those nanodomains change during deformation. The FOSA nanodomains are similar to the self-assembled cores of block copolymer micelles, where SANS using contrast matching techniques has been used to understand the chain exchange kinetics between micelles.[16] In this case, chain exchange of the free micelles is driven by thermal energy fluctuations (kT) that

Received: December 11, 2016
Revised: January 16, 2017
Published: February 9, 2017

DOI: 10.1021/acs.macromol.6b02680
Macromolecules 2017, 50, 1672−1680

allow chain expulsion/insertion between micelles. More recently, Peters and Lodge[17] studied the rheological relaxation behavior of the same triblock block copolymer (BCP) when swollen by a solvent that is selective for the midblock of the BCP. The characteristic relaxation time was nearly 4 orders of magnitude faster than that for the thermally induced chain exchange.[17] Those results demonstrate the importance of stress-driven relaxation processes with regard to the properties and structure of supramolecular networks.

Herein, we describe the structural changes within a DMA/FOSA physical hydrogel containing 9.7 mol % FOSA (denoted as DF10) by *in situ* SANS measurements during stress relaxation in a 150% step-strain experiment. The structural changes of the FOSA nanodomains and the elastic DMA (network) chains that bridge the nanodomains were resolved by contrast matching SANS techniques. Immediately after stretching, the scattering pattern associated with the nanostructure became anisotropic, but relaxed toward the isotropic state during the stress relaxation when the sample was held at a constant macroscopic strain of 150%. The relaxation times associated with the stress and structure relaxations were measured and compared to attain an understanding of how stress relief is related to changes in the hydrogel microstructure when the sample is held at a fixed strain.

EXPERIMENTAL SECTION

Materials. *N*,*N*-Dimethylacrylamide, (DMA, 99.9%, Sigma-Aldrich), 2-(*N*-ethylperfluorooctanesulfonamido)ethyl acrylate (FOSA, 95% BOC Sciences), azobis(isobutyronitrile) (AIBN 99.9%, Sigma-Aldrich), 1,4-dioxane (99.5%, Sigma-Aldrich), diethyl ether (99.5%, Sigma-Aldrich), methanol (99.5%, Sigma-Aldrich), and D_2O (99.5%, Cambridge Isotope Laboratories) were purchased and used as received unless otherwise noted. The DMA was purified by distillation under vacuum, and the FOSA was purified by recrystallization in methanol prior to polymerization.[18] Milli-Q water (18.2 MΩ) was used for H_2O in all studies.

A random copolymer was synthesized by the free radical polymerization of DMA and FOSA using a monomer-to-initiator (AIBN) ratio of 1000 to 1. The reactivity ratios for DMA and FOSA have been reported to be near unity,[19] and thus the monomers incorporated randomly. The monomer mixture of DMA and FOSA was first sparged with N_2 for 1 h, and then the AIBN, dissolved in 5 mL of 1,4-dioxane, was injected into the solution through the rubber septum. To initiate the polymerization, this mixture was heated to 60 °C and then continuously stirred for 24 h. The reaction was terminated by exposure to air, and then the mixture was cooled to ambient temperature. The polymer solution was concentrated by rotary evaporation and subsequently precipitated in an excess of diethyl ether. The composition of the copolymer was determined by ^{1}H NMR (Varian Mercury-300) to be 9.7 mol % FOSA (Figure S1). The molecular weight of the copolymer was 67 kDa with $Đ$ = 1.97 as determined from GPC (Waters 1515 HPLC with a Waters 2414 refractive index detector) using THF as the eluent and calibrated against polystyrene standards.

Stress Relaxation Measurements. In order to fabricate the hydrogels, the vacuum-dried copolymer was compression molded under vacuum at 165 °C and hydrated in Milli-Q water for at least 7 days, which was found to be sufficient for the copolymer to reach its equilibrium swelling in water. Dogbone-shaped hydrogel samples (40 mm × 34 mm with 20 mm × 20 mm gauge section) were cut from the swollen sheet for mechanical testing. The stress relaxation was determined using a TA.XT Plus Texture Analyzer (Stable Micro Systems) at an extension rate of 400 mm/min to 150% gauge strain, the sample was held at this strain, and the stress decay at constant strain was subsequently monitored for 2 h. The sample hydration was maintained during the stress relaxation measurement by spray application of water inside of a sealed flexible chamber. For strain to break measurements, the same dogbone samples were used with an extension rate of 30 mm/min until failure.

Time-Resolved SANS Measurements. For SANS measurements, these same dogbone hydrogel samples were soaked in D_2O/H_2O mixtures (accounting for the H_2O already present in the hydrogel) for 48 h to allow D/H exchange to obtain the desired contrast in the system. In this case, the stretching stage was a simple extension stage composed of two flat plate clamps that has previously been reported for wrinkling experiments[20] and enabled the strain to be applied and held during the duration of the scattering experiments. The sample was stretched to the desired strain (150%) in approximately 5 s, and then the stage was locked in place to maintain a constant strain for the experiment. The entire stretching stage was placed in a large sealed chamber with two large openings covered with aluminum foil to allow transmission of the neutron beam. Images of the stretching stage and the humidity chamber are provided in the Supporting Information. Inside the container, the appropriate D_2O/H_2O mixture to match the sample was added, and the sides of the container were lined with paper towels, which were moistened in the D_2O/H_2O mixture on the bottom. These paper towels increased the surface area for water evaporation to maintain a high humidity level in the chamber, which minimized evaporation from the sample. The SANS measurements were initiated approximately 3 min after stretching the DF10 sample to 150% due to the time required to load the sample into the chamber and align it on the beamline.

SANS measurements were performed on the NGB 30 m beamline at the Center for Neutron Research at the National Institute of Standards and Technology (Gaithersburg, MD).[21] A wavelength, λ, of 5 Å with a wavelength spread, $\Delta\lambda/\lambda$, of 14% was used for all measurements with a rectangular beam (1 cm wide × 1.5 cm tall). This beam dimension was selected to maximize the neutron flux and ensure that the beam did not scatter from edges of the sample. Initially, the hydrogels were measured in the unstretched state. For these static measurements, a broad scattering vector ($Q = 4\pi\lambda \sin\theta$, where θ is the scattered angle) range was examined with three sample-to-detector distances: 1.33 m (eight beam guides), 4 m (four beam guides), and 10.5 m (one beam guide). This larger Q range was examined to determine the best sample-to-detector where the critical features associated with the scattering from the DF10 hydrogel can be resolved. The wider Q range scattering profiles are shown in Figures S2 and S3 for both contrasts examined. For the time-resolved measurements, the sample-to-detector distance was 1.33 m with eight beam guides used. This distance was selected as the primary correlation peaks are well resolved in the associated Q-range. The scattering data were averaged over 180 s for the first 30 min of the relaxation and then over 300 s for longer times to improve the statistics when the structure was not changing as rapidly.

The 2D scattering data were reduced to absolute intensity accounting for the beam intensity, detector sensitivity, sample thickness, and sample transmittance using the methods outlined by Kline and co-workers with Igor Pro software.[22] Because of the anisotropy in the scattering that developed from the stretching, the 2D scattering data were azimuthally averaged to obtain 1D profiles using sector averages with a width of ±22° that were centered either parallel (90° azimuthal) or perpendicular (0° azimuthal) to direction of stretching (Figure S4). The scattering peak in these 1D profiles were fit using the broad peak model[23] for both contrasts. The anisotropy in the scattered intensity was quantified using an annular Q average about the scattering peak position to yield intensity as a function of azimuthal angle. The Q-range for this averaging was selected to be the full width at half-maximum (fwhm) of the scattering peak of the initial unstretched samples. For the hydrogel swollen with 27/73 (v/v) D_2O/H_2O, the averaging was performed over the $\Delta Q = 0.092 \pm 0.024$ Å^{-1}, while $\Delta Q = 0.14 \pm 0.047$ Å^{-1} was the range for the averaging of the intensity for the hydrogel with 50/50 (v/v) D_2O/H_2O.

RESULTS AND DISCUSSION

The chemical structure of the DF10 copolymer and a schematic of the microstructure of the DF10 hydrogel[13] are shown in

DOI: 10.1021/acs.macromol.6b02680
Macromolecules 2017, 50, 1672−1680

Figures 1A and 1B, respectively. The network cross-link junctions were the core−shell nanodomains formed by

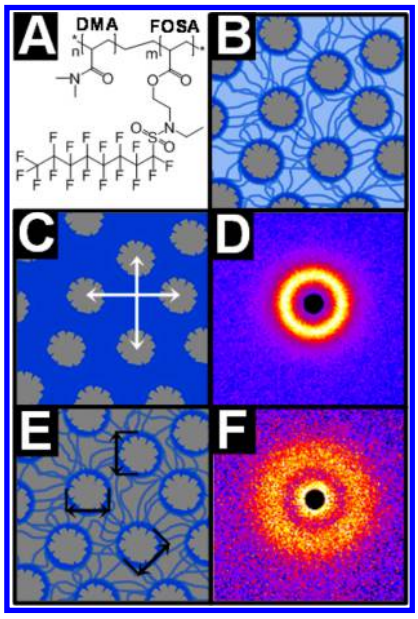

Figure 1. (A) Chemical structure of DMA-FOSA and (B) schematic representation of the DF10 hydrogel nanostructure that consists of FOSA aggregates (gray) surrounded by a water-depleted DMA phase (dark blue) dispersed in a continuous hydrated DMA phase. Schematic of the structure resolved by SANS using D_2O/H_2O mixture to contrast match (C) DMA (27/73 (v:v) D_2O/H_2O) and (D) the 2-D SANS pattern to determine the interdomain spacing, D. Schematic of hydrogel structure when (E) FOSA is contrast-matched (50/50 (v:v) D_2O/H_2O) and (F) the associated 2-D SANS pattern to determine the nanodomain size, ξ, from the form factor associated with the shell structure. The hydrogels were measured at ∼23 °C in the unstretched state.

aggregation of the hydrophobic FOSA. Despite the random nature of the copolymer, these aggregates of the FOSA are relatively uniform in size. This behavior is similar to a recent report by Hirai et al. where uniform micelles were formed from amphiphilic random copolymers.[24] In this case, the density of the FOSA aggregates is sufficient to form a network in water, which leads to a mechanically stable hydrogel. The schematic of the hydrogel in Figure 1B is color-coded to the chemistry of the hydrogel where the FOSA core of the nanodomains are represented in gray, DMA in dark blue, and the water in light blue. The water-depleted shell is composed of predominately DMA segments within approximately 1 nm of the FOSA core, so the FOSA domains are surrounded by the dark blue of DMA. The DF10 hydrogel exhibits a swelling ratio (mass hydrogel/mass dry polymer) of 3.3, which suggests approximately 10 vol % of the continuous phase is DMA chains with the remainder water. This DF10 hydrogel could be elongated over 400% before failure (Figure S5). From a characterization perspective for the structure determination, the large difference in the scattering length density (SLD) between hydrogen and deuterium enables the SLD of the DMA or FOSA phase to be contrast matched with mixtures of H_2O/D_2O.[25] Contrast matching allows one to resolve the scattering from just the FOSA phase using an aqueous mixture of 27/73 (v/v) D_2O/H_2O, which matches the SLD of the DMA (Figure 1C). When the hydrogel is hydrated with 27/73 (v/v) D_2O/H_2O, the scattering is dominated by the core of the nanodomain composed of FOSA as the matrix of the hydrogel contains DMA and D_2O/H_2O with the same SLD. In this case, the shell around the FOSA nanodomains is not visible as the aqueous phase matches the DMA.

Figure 1D shows the 2-D isotropic scattering from the DMA contrast matched system prior to any deformation. This scattering profile is consistent with the structure illustrated schematically in Figure 1C. This scattering provides the structure factor associated with an average interdomain spacing between the FOSA aggregates, D = 6.95 nm, for an unstretched DF10 hydrogel at ∼23 °C. This spacing, D, is schematically shown by the arrows in Figure 1C. The intensity of the peak is related to the number density of domains with the same spacing and the width of the scattering peak is indicative of the breadth of the distribution of these interdomain spacings.

In a similar vein, the DMA can be independently resolved using a mixture of 50/50 (v/v) D_2O/H_2O to match the SLD of the FOSA. Figure 1E schematically illustrates the structure of the hydrogel gleaned from this contrast. The aqueous phase contains ∼10 vol % DMA chains that comprises the continuous phase of the hydrogel, which are now visible to the neutrons as the water has the same SLD as FOSA and is thus gray in the schematic. The water-depleted shell surrounding the FOSA core is also highlighted, as the SLD for the shell is approximately that of pure DMA and is thus shown as dark blue. As the shape and size of the nanodomains are well-defined, the scattering is dominated by the form factor from the water-depleted shell of the nanodomain (Figure 1F).

Figure 1F shows the isotropic 2-D scattering pattern when the FOSA is contrast matched by 50/50 (v:v) D_2O/H_2O, as illustrated schematically in Figure 1E. This scattering pattern includes contributions from the form factor of the DMA network chain, but the scattering is dominated by a peak that arises from the intrashell correlation from the form factor associated with the core−shell contrast of the water-depleted DMA layer surrounding the FOSA core. This peak in the scattering from the form factor occurs due to the shell having an SLD that is significantly smaller than that for the core and matrix. A similar scattering behavior has been previously reported for selectively labeled dendrimers, which leads to a similar shell−core structure in solution.[26] In Figure 1F, the peak location is directly related to the size of the nanodomains, ξ = 4.53 nm, which is the diameter of the FOSA core plus the thickness of the water-depleted DMA shell. ξ is hereafter used to describe the nanodomain size. The arrows in Figure 1E illustrate ξ schematically.

In addition to understanding the structure of the hydrogel in the undeformed state, the stress relaxation behavior of the DF10 hydrogel is another baseline requirement to enable insight into the relationship between nanoscale structure and relaxations that lead to high toughness of these hydrogels. For the stress relaxation, the DF10 hydrogel was extended rapidly (400 mm/min) to 150% strain as shown in Figure 2A. The stress relaxation was then monitored for 2 h, while ensuring the sample remained hydrated by using a humidity chamber. Figure 2B shows that about 60% of the stress relaxed in the first 2 min and ∼80% of the stress relaxed within the first 20 min. During the next 100 min, the stress relaxed to ∼7% of the initial load.

Stress relaxation data are commonly described by a stretched exponential function, which has been shown to provide a reasonable fit of stress relaxation data for the DMA−FOSA copolymers,[27] but these relaxation measurements are generally performed at low strains.[28] A stretched exponential, however,

DOI: 10.1021/acs.macromol.6b02680
Macromolecules 2017, 50, 1672−1680

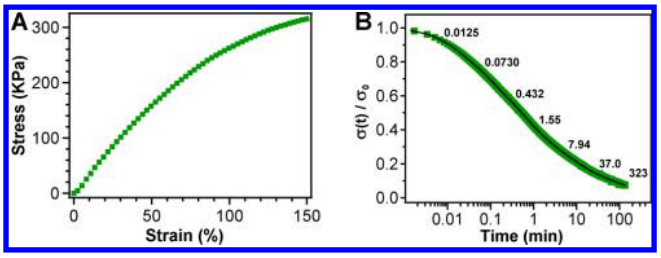

Figure 2. (A) Stress−strain behavior associated with the extension of the DF10 hydrogel to 150% strain at 400 mm/min. (B) Stress relaxation of DF10 at a constant applied 150% strain. The solid line is the fit of a generalized Maxwell model with seven elements. The calculated relaxation times are listed above the fit curve at approximately the relaxation time.

provides only an average relaxation time and a measure of the breadth of the relaxation time distribution. That weakness is especially important with regards to multiphase systems, such as the DMA−FOSA hydrogels, where there may be multiple structures that have their own distributions of relaxation times. An alternative approach for fitting stress relaxation data, used herein, is to employ a generalized Maxwell model (GMM),[29] eq 1, that provides multiple relaxation times, but it also requires a more complex mathematical fit of the experimental data (additional fit parameters)

$$\frac{\sigma(t)}{\sigma_0} = \sum_{n=1}^{N} A_n e^{-t/\tau_n} \quad (1)$$

where $\sigma(t)$ is the instantaneous stress, σ_0 is the initial stress (t = 0), τ_n is the relaxation time of the nth Maxwell element, A_n is an apportioning factor of how much each Maxwell element contributes to the total stress, and N is the number of Maxwell elements needed to describe the stress relaxation data. A GMM with N = 7 fits the stress relaxation data for the DF10 hydrogel well (see black line in Figure 2 and residual error of fit in Figure S6), with relaxation times of τ_n = 0.0125, 0.0730, 0.432, 1.55, 7.94, 37.0, and 323 for n = 1−7, respectively. Note that the relaxation times span 5 orders of magnitude. The choice of 7 relaxation times was arbitrary, but the fit was not significantly improved when N > 7. The GMM fits for N = 1−6 and the associated residual error of the fit are shown in Figure S7.

Figure 3 shows both the SANS 2D scattering profiles and the 1D profiles for the average scattering intensity across the peak as a function of azimuthal angle for step-strain experiments that match the stress relaxation experiment (Figure 2). The stretch direction for the sample corresponds to the arrows in the 2D scattering plots in Figure 3. Figure 3A illustrates the scattering using a hydrogel with a 27/73 (v:v) D_2O/H_2O mixture. In this case, the peak position in the 2D scattering is related to the interdomain spacing (D) between the FOSA aggregates. Shortly after stretching (4 min), the scattering profiles show a higher intensity on the ring along the equator (at ϕ = 0° and 180°). The differences in the azimuthal scattering intensity are related to the concentration of the nanodomain correlations in the directions perpendicular versus parallel to the stretching direction. This anisotropy can be better illustrated by the 1D patterns where the average intensity of the peak, centered at Q = 0.092 Å^{-1} and averaged over ΔQ = 0.024 Å^{-1}, for the interdomain scattering is examined as a function of azimuthal angle. In Figure 3A, there is a clear peak in the scattered intensity at ϕ = 0° and 180° at 4 min. At intermediate time (24 min), the azimuthal variance in intensity decreases, but a maximum in intensity remains at ϕ = 0° and 180°. At long times (424 min), the average intensity across the peak is independent of azimuthal angle, which indicates that the anisotropy in the concentration of the nanodomain correlations imparted by the step strain has relaxed over the time frame of the SANS experiment.

Figure 3B illustrates the scattering using a hydrogel with a 50/50 (v:v) D_2O/H_2O mixture. Here, the peak position in the 2D scattering is related to the nanodomain size (ξ) that was determined from the intrashell correlation peak ($\xi = 2\pi/Q_0$) associated with the contrast for the core−shell structure of the nanodomain. The 1D scattering patterns in Figure 3B are averaged by integration over the width of the peak at Q = 0.14 ± 0.047 Å^{-1}. Similar to the scattering from the FOSA nanodomain correlations (structure factor), the scattering patterns associated with the form factor of the nanodomain also became anisotropic on deformation as shown in Figure 3B. From the azimuthal dependent intensity, the peak (associated with the anisotropy in intensity) is much broader for the scattering associated with the nanodomain shape (Figure 3B) in comparison to the FOSA nanodomain correlations (Figure 3A)

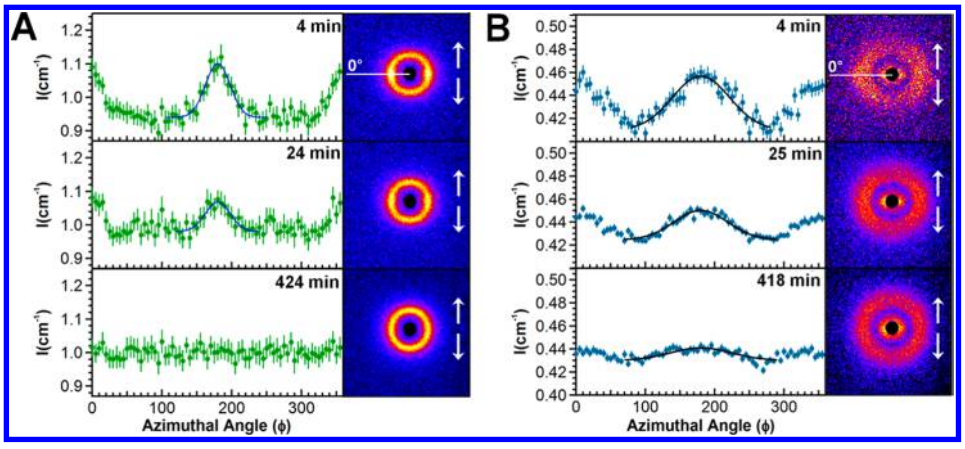

Figure 3. Time-resolved 2D SANS profiles and azimuthal angle dependence of the average intensity of the peak at 4, ~25, and ~420 min after the step strain to 150% to examine (A) the interdomain distance measured from FOSA scattering (DMA contrast match) where the intensity is averaged over Q = 0.092 ± 0.024 Å^{-1} and (B) the shell size from DMA scattering (FOSA contrast match) where the intensity is averaged over Q = 0.14 ± 0.047 Å^{-1}. The ϕ = 0° azimuthal angle is shown on the first 2D pattern of each set of data for reference.

DOI: 10.1021/acs.macromol.6b02680
Macromolecules 2017, 50, 1672−1680

after 4 min of relaxation. The difference in the scattered intensity, associated with the directions parallel and perpendicular to the stretching, decreases as the sample relaxes. However, a discernible peak in the azimuthal dependence of the scattered intensity remains even after 418 min that is associated with the form factor (shape) of the nanodomains. To more clearly illustrate the anisotropy in the scattering, the intensity scale for the 2D scattering patterns has been rescaled for both contrasts (Figure S8). In order to explain the anisotropy in the intensity, which is associated with the concentration of the water-depleted DMA shells, the physics of the processes involved during a large step deformation must be considered. In the stretching direction, the DMA tie chains will become extended leading to deformation of the FOSA nanodomains and ultimately pull out of FOSA moieties from the nanodomains. This pull-out will disorder the DMA shell and likely lead to hydration of the DMA to reduce the scattering contrast associated with the shell. However, the scattering intensity associated with the shell does not fully recover over the time frame of these SANS experiments (7 h). As this scattering is associated with the water-depleted DMA, it is instructive to examine the scattering more carefully to extract information associated with the DMA chain conformation. The 2D scattering profiles for the stretched hydrogel (Figure 3B) exhibited a butterfly pattern near the beam stop, which is characteristic of chain stretching[30−33] in the direction parallel to the strain. This butterfly pattern is not present in the unstretched hydrogel (Figure 1F). When examining the temporal evolution of the 2D scattering patterns, the butterfly pattern persisted through the entire experiment, which indicates either a permanent deformation of the DMA chains (residual stress on the interconnecting DMA chains) or that relaxation of the DMA chains was not complete after 7 h. As the hydrogel remains in a strained state (150%) at the completion of the SANS measurements, the limited shape recovery (~20% decrease in the length of the hydrogel) on release of the hydrogel from the clamps provides some evidence for residual stresses remaining in the material. The deformed DMA chains that give rise to the butterfly pattern at the end of the relaxation experiment likely provides some of the retractive force to decrease the length of the hydrogel. The long recovery for these DMA chains could be associated with the glassy nature of the FOSA core, which significantly reduces the ability for FOSA monomers to rearrange their location.

To more quantitatively examine the anisotropy in the scattering intensity, the peaks in the azimuthal angle dependent intensity (Figure 3) were fit with a Gaussian function (solid lines). The amplitude of the Gaussian peak (difference from maximum intensity to baseline intensity) provides a measure of the relative anisotropy in the system. For direct comparison to the stress relaxation data, this Gaussian peak amplitude at any time, t, was normalized by the amplitude instantaneously upon stretching, $t = 0$, to provide quantification of scattering anisotropy in terms of an amplitude ratio, AR $\equiv A(t)/A_0$. However, since the first SANS measurement was obtained at $t = 4$ min after stretching, the actual value of A_0 is not directly measured. In order to estimate A_0, the amplitude determined from the Gaussian fit of the peak in $I(\phi)$ was plotted as a function of time and fit with the sum of three exponential functions (Figure S9)

$$A(t) = \sum_{n=1}^{3} \alpha_n e^{-t/\beta_n} \quad (2)$$

where the α_n and β_n are constants. The sum of three exponentials produced an excellent fit of the data, and the value of A_0 was then determined by using the regression equation to extrapolate the data to $t = 0$. That introduces some error in the absolute value of AR, but the relative changes in AR are the important factor to consider here, so this extrapolation is not seen as a critical deficiency of the analysis described below.

Figure 4 shows how the AR, which is a measure of the anisotropy in the scattering intensity of the peak, decays during

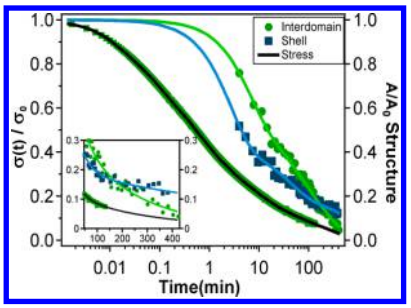

Figure 4. Time dependence of the stress and intensity anisotropy measured by SANS during stress relaxation following a step strain. The green-circles data correspond to the normalized amplitude ratio for the azimuthal peak associated with I_D (DMA was contrast matched), and the blue-squares data correspond to the normalized amplitude ratio for the azimuthal peak data for I_ξ (FOSA was contrast matched). The solid lines provide a GMM fit of the structural relaxation. The solid black curve is the GMM fit of the stress relaxation data reproduced from Figure 2 with the stress data shown as the green squares. The inset shows the same data on a linear time scale.

stress relaxation following a step strain to 150%. It should be noted that here we are only describing the anisotropy in the averaged scattering intensity of the correlation peaks associated with either the interdomain spacing (I_D) or the intradomain size (I_ξ). AR does not include any information about the dimensions associated with the spacing or size (correlation peak position) as I_D and I_ξ are averaged across the width of the correlation peak. For both contrasts, there was first a rapid decay in the anisotropy of the scattering intensity. The AR decayed to 50% of its initial value in ~4 min for I_ξ and ~15 min for I_D, which infers a relatively rapid structural recovery for a majority of the DF10 hydrogel. At these short relaxation times, the structural relaxation processes associated with the anisotropy in the intensity of the two phases of the hydrogels are suspected to be correlated due to the glassy nature of the FOSA domains, which should limit the kinetics of structural recovery. For I_D, the changes in AR are associated with recovery of nanodomains with a spacing of approximately D and the reformation of the water-depleted DMA around the FOSA nanodomains to provide contrast for scattering. At longer times, the relaxation of the scattering associated with spacing of the FOSA nanostructure, I_D, diverged from that associated with the anisotropy of the shell scattering, I_ξ. The former decayed to zero, while the anisotropy associated with the water-depleted DMA shell relaxed very slowly, and I_ξ remained finite after 7 h.

The rate of the decay in the anisotropy in the scattered intensity for the two contrasts examined provides some insight into relative mobility of the two phases of the hydrogel and the

DOI: 10.1021/acs.macromol.6b02680
Macromolecules 2017, 50, 1672−1680

differences in the structural relaxation processes. The interdomain spacing, D, is dependent on the conformation of the DMA chains that connect the nanodomains. Stretching the hydrogel and orients the *network* chains in the direction of elongation. That also produces a restoring force in the DMA chains in accordance with rubber elasticity. The continuous, water-swollen DMA phase is primarily water, so the network chains have considerable mobility, which generates a relatively fast stress relaxation process to restore a uniform density of nanodomains, which corresponds to a decay of A/A_0 to zero, which matches the unstretched, isotropic hydrogel.

The intrashell correlation from the form factor of the nanodomains, ξ, provides the approximate nanodomain size. This correlation is a result of the water-depleted DMA shell surrounding the glassy FOSA nanodomain as has been reported previously.[13,14] The intrashell correlation is affected in two ways by stretching the hydrogel. First, the nanodomains can undergo a solid-like deformation, but this does not impact I_ξ, which defines the AR, but rather impacts the relative position of the scattering peak. The retractive stress in the attached network chains can reorient the nanodomains to relax this stress. Second, the stress from the network chains may rearrange the FOSA groups in the nanodomain core to pull FOSA groups out of the nanodomain, which produces stress relaxation. This pull-out would likely hydrate the DMA segments near the FOSA and thus impact I_ξ. Removal of a perfluorinated FOSA group from the nanodomain into the water-swollen polymer phase, however, produces a large enthalpic penalty, so there is a significant driving force for the reaggregation of the FOSA into either the original nanodomain or an adjacent nanodomain. Since the nanodomains are glassy, the relaxation times of the aggregated FOSA groups in the core and of the DMA segments in the shell are expected to be large. Thus, once the stress in the continuous water-swollen DMA phase has mostly dissipated, such that the energy associated with the residual stress is less than the enthalpic penalty associated with removal of a FOSA group into the aqueous phase, one might expect little further structural relaxation of the nanodomain anisotropy, which is consistent with the slow relaxation of the remaining intrashell scattering, I_ξ, shown in Figure 4 at the long times.

In order to better compare the structural relaxations with the stress relaxation, the decay of the anisotropy in I_D and I_ξ were each fit with the sum of three exponentials

$$\frac{A(t)}{A_0} = \sum_{n-1}^{3} A_n e^{-t/\tau_n} \quad (3)$$

where the A_n provide the relative contributions of each relaxation process and the τ_n are relaxation times. The choice of three exponentials was arbitrary and was solely based on the fact that three exponentials fit the data better than two and using four exponentials did not significantly improve the fit, but this follows the GMM used to fit the stress relaxation. The relaxation times generated from the structure relaxation fits, 6.28, 47.3, and 252 min and 2.63, 42.1, and 950 min for I_D and I_ξ, respectively, show the longer time relaxation behavior of the nanodomains. Note that the two shorter relaxation times for both structure relaxations were similar, which is due to the connectivity of the two structures. That is, the shorter time relaxation processes of the nanodomain anisotropy were coupled to the relaxation of the network chains. However, once the network chain relaxed (τ = 252 min), the driving force for relaxation of the nanodomain structure was essentially removed, which explains the much longer relaxation time (τ = 950 min) for the anisotropy associated with the water-depleted DMA shell that persisted for over 7 h. The continued relaxation of the nanodomain correlation anisotropy after the network chains had relaxed may be a consequence of thermal processes, similar to what has been reported for the relaxation of structure in block copolymer micelles.[16]

In addition to the anisotropy of the scattering peak intensities, I_D and I_ξ, the location of the scattering peak, which is related to the spacing, D, or size of the nanodomains, ξ, changed on stretching in a manner dependent on the direction relative to the applied deformation. During the stress relaxation, the spacing and size also generally relaxed with time toward the dimensions for the unstretched, isotropic hydrogel. In order to analyze these dimensional changes, the 2D scattering profiles (see Figure 1 for examples) were converted to directional 1-D plots by using an azimuthal (ϕ) sector average to yield $I(Q)$ for the scattering primarily parallel (ϕ = 90 ± 22°) and primarily perpendicular (ϕ = 0 ± 22°) to the stretching direction. An example of these azimuthal sector averages is shown in Figure S10. Those scattering profiles provided the scattered intensity as a function of Q and thus provide a route to obtain the average interdomain distance, D, or nanodomain diameter, ξ. $I(Q)$ was fit using a broad peak model[22,23] to determine the peak position (D and ξ) and full width at half-maximum (fwhm). The fwhm provided a measure of the distribution of D and ξ. The temporal dependences of D and ξ provide insight into how the nanodomains and network chains (interdomain distances) deform when the sample was stretched and during the stress relaxation process as shown in Figure 5.

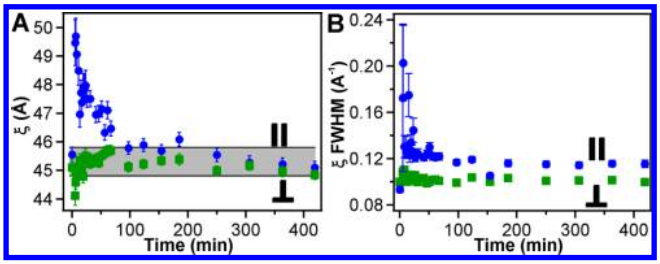

Figure 5. (A) Evolution of ξ (nanodomain size) in the parallel (∥) and perpendicular (⊥) directions to the deformation during relaxation. (B) The fwhm of the scattering peak associated with ξ that describes the change in the distribution of sizes.

Figure 5A shows that at 4 min after the step-strain (i.e., the earliest SANS data that were obtained) the FOSA nanodomains were stretched by nearly 5 Å (11.5%) parallel to the stretching direction and simultaneously compressed by 1.5 Å (3.4%) perpendicular to the stretching direction. The difference in the deformation of the nanodomain parallel and perpendicular to the stretching direction is consistent with the Poisson's ratio expected for a glass (≈1/3). This infers that the density of the nanodomains is decreased under tension (dilative deformation). In less than 100 min, the nanodomain size, ξ, in both directions recovers to its original value, with $\xi_\perp$ appearing to recover more quickly. It is important to note that the anisotropy in the sizes of the nanodomains decays to isotropic (Figure 5) much faster than the long-lived anisotropy in the scattered intensity (I_ξ) that was determined as a function of azimuthal angle (Figure 4). This difference can originate with the origin of the scattering peak associated with ξ, which is the

DOI: 10.1021/acs.macromol.6b02680
Macromolecules 2017, 50, 1672−1680

form factor for the water-depleted DMA shell surrounding the FOSA nanodomains. For the size ξ, only the peak location (Q) is important, and small variation in the contrast will not impact the calculated size of the nanodomain. Conversely, the intensity of the peak (I_ξ) is directly related to the contrast in the system and the number of nanodomains of similar size, so alteration of the distribution and hydration level of connecting DMA chains near the FOSA nanodomains may have occurred that would impact the scattered intensity, but not the location of the correlation peak.

In addition to the size of the nanodomain, the breadth of the correlation peak provides information about the distribution of sizes as quantified by at the fwhm shown in Figure 5B. Upon stretching, the fwhm in the direction parallel to the deformation is nearly double its isotropic value, with larger error bars. This would suggest the nanodomain is highly distorted in the direction of the stretching with a large distribution of sizes in the parallel direction. The large uncertainty in the fit arises from the decreased scattered intensity, which may be associated the nature of the water-depleted shell. Again by 100 min, the distribution (fwhm) has nearly recovered similar to the recovery for ξ, but the fwhm in the parallel direction of strain remains larger than its initial isotropic value. This behavior aligns with Figure 4, which indicates that the scattered intensity associated with the shell (I_ξ) remains slightly perturbed and is not able to fully recover. The slightly broader distribution of sizes of the nanodomains is likely indicative of the distribution of stresses imposed to the nanodomains that result in plastic deformation as their glassy nature should inhibit significant rearrangements beyond elastic recovery. This deformation could be accompanied by an altered distribution and hydration level of connecting DMA chains near the FOSA nanodomains in the direction parallel to the stretching. In contrast, the perpendicular direction fwhm for the nanodomain size remains largely unchanged throughout the relaxation, which suggests that the changes in $\xi_\perp$ perpendicular to the applied deformation are likely limited to relatively uniform deformation of the FOSA nanodomains. The difference in the behavior of the fwhm in the directions parallel and perpendicular to the stretching may be a result of FOSA pull-out into the aqueous phase under tension (parallel) that alters the distribution of nanodomain sizes if the FOSA is subsequently inserted into a neighboring domain.

Figure 6A shows how the interdomain distance, D, evolves during the stress relaxation. As our first measurement is made at 4 min, we are unable to fully capture the initial structural relaxation immediately on stretching. Upon stretching the sample, the interdomain distance parallel to the stretching direction, $D_\parallel$, initially increased, and the interdomain distance perpendicular to the stretching direction, $D_\perp$, initially decreased in the first few minutes. These dimensional changes in the spacing between the nanodomains are qualitatively consistent with expectations associated with the uniaxial stretching based on bulk dimension changes on deformation. However, the initial increase of $D_\parallel$ and decrease of $D_\perp$ were followed by a rapid change in the two spacings that led to an increase of $D_\perp$ by 1.4 Å from D_0 (unstrained sample) and a decrease of $D_\parallel$ by 1.4 Å. The decrease in $D_\parallel$ persisted for over 7 h. There was no statistical difference between the spacing at 100 and 420 min. This lack of recovery of $D_\parallel$ to its initial dimensions is similar to the persistence of the butterfly pattern associated with stretched DMA chains (Figure 3B). As the hydrogel remains macroscopically strained to 150% during the stress relaxation, it is not

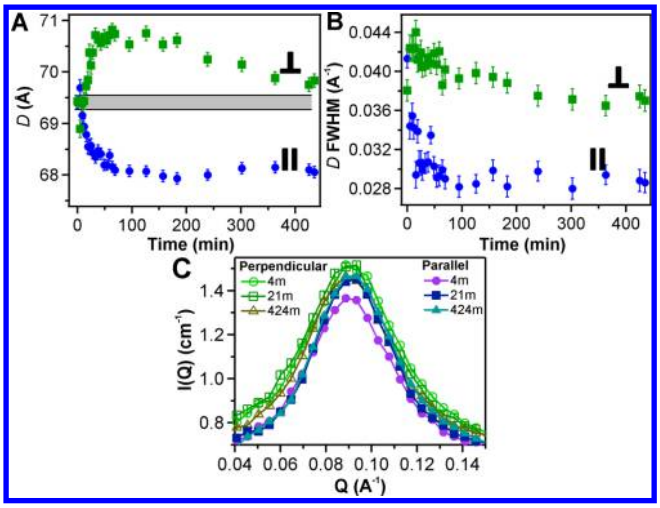

Figure 6. Temporal evolution in (A) D (interdomain spacing) upon stress relaxation and (B) fwhm of the scattering peak both parallel (∥) and perpendicular (⊥) to the deformation. The gray area represents isotropic interdomain distance before strain within one standard deviation. The fwhm provides a measure of the distribution of D distances. (C) $I(Q)$ near the interdomain scattering peak for several relaxation times both parallel (∥) and perpendicular (⊥) to the deformation. These scattering profiles reveal the asymmetric rearrangement of D showing a significant loss on the low Q (larger spacing) side in parallel direction.

unreasonable that the structure does not recover to its original state. In the perpendicular direction, $D_\perp$ increased to a maximum of 71 Å, but then began to relax back toward the initial dimensions of the unstrained sample at ≅100 min. The spacing then slowly decayed over the next 300 min back D_0 of the DF10 hydrogel. Note that the time at which $D_\perp$ began to diminish coincided with the time at which ξ returned to its initial, unstretched value (cf. Figures 5A and 6A).

The initial increase in $D_\parallel$ and initial decrease in $D_\perp$ are consistent with expectations for the change in the spacing between cross-links on a stretching deformation as is the relaxation toward the initial interdomain spacing, D_0. However, it is not readily apparent how and why $D_\parallel$ decreases to less than D_0 (and $D_\perp$ increases beyond D_0) during the initial relaxation. This behavior appears to be almost an oscillation in the deformation and may be related to the recoil of the chains on relaxation. This overshoot in the recovery may be related to the initial step strain applied, through the amount of potential energy transmitted to the network chains. Determining the mechanisms associated with the overshoot in the structural recovery requires additional study.

Nonetheless, the distribution of D through the fwhm provides some preliminary insights into this behavior. As shown in Figure 6B, the fwhm, which corresponds to the distribution of D parallel to strain, decreases by 25%, so the interdomain spacing becomes better defined after the stretching. This decrease in fwhm is counter to the increase in the distribution associated with ξ (Figure 5B). The fwhm parallel to the stretching direction does not recover in the 7 h of the measurement, similar to how the spacing changes plateau at a lower D (Figure 6A) in this direction. In order to understand how the fwhm on recovery can be smaller than the initial fwhm of the unstretched hydrogel, $I(Q)$ near the peak is examined for several times as shown in Figure 6C. The scattering profiles are nearly invariant qualitatively when

DOI: 10.1021/acs.macromol.6b02680
Macromolecules 2017, 50, 1672−1680

examining the direction perpendicular to the stretching, which is consistent with the analysis from the fit of these data in terms of D (Figure 6A) and fwhm (Figure 6B). Conversely, there is a clear change in the shape of $I(Q)$ in the parallel direction to the stretching with an asymmetric change in the shape of the peak as intensity decreases on the low Q side of the scattering peak, which corresponds with a decrease in the number of nanodomains with a larger than average D. This scattering profile does not appreciably change between 17 and 420 min, but there is a large change from 4 to 17 min with an increase in the total scattering intensity at longer times. To explain the loss of the low Q side of the scattering peak on stretching, one would expect that most extended network chains, which should correspond to the larger D, are more efficient at transferring stress to the nanodomains to lead to preferential pull-out of FOSA groups attached to these extended network chains during stretching. The larger spacings between the nanodomains do not appear to re-form upon relaxation of the stress in the network. On relaxation, one could imagine that there is a probability distribution associated with DMA chain conformation that also controls the spacing between the nanodomains. As such, there is likely a greater probability to re-form cross-links with a less extended state for the connecting chains as the extended chains were preferentially removed during the stretching process.

One additional possibility to explain these results is the change in the volume of the hydrogel during the stretching and relaxation process. At low strains, hydrogels are generally treated as rubbers with a Poisson's ratio of 1/2, which leads to isochoric deformation. As the initial deformation is large (150% strain), the mechanical response is likely nonlinear, and Poisson's ratio likely changes during the experiment as has been reported for other hydrogel systems.[34] A Poisson's ratio less than 1/2 leads to a reduced density for the material after deformation. During the stress relaxation, the FOSA nanodomains that comprise the cross-links and DMA network chains rearrange and this reorganization at a reduced density when initially stretched may also act to alter the equilibrium structure after relaxation. These SANS experiments exploring the structural evolution in a hydrophobically cross-linked hydrogel only begin to reveal how the reversible cross-links relax in response to a tensile step strain. Understanding of nonlinear mechanics associated with reversibly cross-linked systems may be assisted by the use of *in situ* scattering experiments that provide insight into structural changes that occur on deformation.

CONCLUSIONS

The structural changes associated with stress dissipation were elucidated in a hydrogel based on an amphiphilic random copolymer of *N*,*N*-dimethylacrylamide (DMA) and 2-(*N*-ethylperfluorooctanesulfonamido)ethyl acrylate (FOSA). SANS and contrast variation enabled the evolution of the structural relaxations to be independently resolved for the two components of the copolymer that comprise the hydrogel. The stress relaxation data following a step strain were fit to a generalized Maxwell model (GMM) with seven elements whose relaxation times spanned 5 orders of magnitude. Structural relaxation was calculated from the anisotropy of the scattering intensity associated with correlation peaks related to the size of the FOSA nanodomains that served as the physical cross-links and the spacing between these FOSA nanodomains. The relaxation times associated with the decay in the anisotropy differed by an order of magnitude and agreed with the longer relaxation times determined from the stress relaxation fits to the GMM.

In addition to the anisotropy in the scattered intensity, the dimensions associated with the size and spacing of the nanodomains also became anisotropic after stretching the hydrogel. On stretching, the interconnecting segments (network chains) initially elongated in the direction of the applied strain, but then rapidly decreased during stress relaxation. The spacing relaxed to dimensions less than that in the unstrained hydrogel. We suspect that this decreased spacing is a manifestation of the preferred stress dissipation from FOSA moieties pulling out of the nanodomains for the most extended DMA tie chains during the stretching process. Even after 7 h of relaxation, the spacing between the FOSA domains remained less than that of the unstretched hydrogel in the direction of the applied deformation. The FOSA nanodomains also deformed anisotropically, but their dimensions quickly recovered to close to those of the isotropic unstretched gel. The results suggested a physical origin for how these nanostructured supramolecular hydrogels dissipate stress through pull-out of FOSA from the nanodomains and their recovery to a structure similar to the initial hydrogel during stress relaxation. These measurements provide insight into the toughening of hydrogels with reversible interactions and their recovery.

ASSOCIATED CONTENT

Supporting Information

The Supporting Information is available free of charge on the ACS Publications website at DOI: 10.1021/acs.macromol.6b02680.

The sector averaging diagram, stress−strain to break curves, stress relaxation GMM model fit residuals, 1−6 GMM models, raw Gaussian amplitude fits, broad peak model fits, distribution changes, and custom cell and humidity cell images (PDF)

AUTHOR INFORMATION

Corresponding Authors

*E-mail rweiss@uakron.edu (R.A.W.).
*E-mail vogt@uakron.edu (B.D.V.).

ORCID

Chao Wang: 0000-0002-5205-9771
R. A. Weiss: 0000-0002-5700-6871
Bryan D. Vogt: 0000-0003-1916-7145

Notes

The authors declare no competing financial interest.

ACKNOWLEDGMENTS

This work was partially financially supported by the Civil, Mechanical and Manufacturing Innovation (CMMI) Division in the Directorate for Engineering of the National Science Foundation, grant CMMI-1300212, and the Chemical, Bioengineering, Environmental and Transport Systems (CBET) Division in the Directorate for Engineering of the National Science Foundation, grant CBET-1606685. This work utilized facilities supported in part by the National Science Foundation under Agreement DMR-1508249. We acknowledge the support of the National Institute of Standards and Technology, U.S. Department of Commerce, in providing the neutron research facilities used in this work. The authors

DOI: 10.1021/acs.macromol.6b02680
Macromolecules 2017, 50, 1672−1680

especially thank Cedric Gagnon (NIST) for his help with setup and configuration of the *in situ* SANS measurements.

REFERENCES

(1) Gong, J. P.; Katsuyama, Y.; Kurokawa, T.; Osada, Y. Double-Network Hydrogels with Extremely High Mechanical Strength. *Adv. Mater.* **2003**, *15* (14), 1155−1158.
(2) Naficy, S.; Brown, H. R.; Razal, J. M.; Spinks, G. M.; Whitten, P. G. Progress Toward Robust Polymer Hydrogels. *Aust. J. Chem.* **2011**, *64* (8), 1007−1025.
(3) Zhai, Y.; Meng, X.; Duan, H.; Ding, Z.; Liu, Y.; Lucia, L. Super Stable and Tough Hydrogel Containing Covalent, Crystalline, and Ionic Cross-Links. *Macromol. Chem. Phys.* **2016**, *217* (1), 32−38.
(4) Agrawal, A.; Rahbar, N.; Calvert, P. D. Strong Fiber-Reinforced Hydrogel. *Acta Biomater.* **2013**, *9* (2), 5313−5318.
(5) Sun, J.-Y.; Zhao, X.; Illeperuma, W. R. K.; Chaudhuri, O.; Oh, K. H.; Mooney, D. J.; Vlassak, J. J.; Suo, Z. Highly Stretchable and Tough Hydrogels. *Nature* **2012**, *489* (7414), 133−136.
(6) Webber, R. E.; Creton, C.; Brown, H. R.; Gong, J. P. Large Strain Hysteresis and Mullins Effect of Tough Double-Network Hydrogels. *Macromolecules* **2007**, *40* (8), 2919−2927.
(7) Nakajima, T.; Kurokawa, T.; Ahmed, S.; Wu, W. L.; Gong, J. P. Characterization of Internal Fracture Process of Double Network Hydrogels under Uniaxial Elongation. *Soft Matter* **2013**, *9* (6), 1955−1966.
(8) Tominaga, T.; Tirumala, V. R.; Lin, E. K.; Gong, J. P.; Furukawa, H.; Osada, Y.; Wu, W.-l. The Molecular Origin of Enhanced Toughness in Double-Network Hydrogels: A Neutron Scattering Study. *Polymer* **2007**, *48* (26), 7449−7454.
(9) Hao, J.; Weiss, R. A. Mechanically Tough, Thermally Activated Shape Memory Hydrogels. *ACS Macro Lett.* **2013**, *2* (1), 86−89.
(10) Myung, D.; Waters, D.; Wiseman, M.; Duhamel, P. E.; Noolandi, J.; Ta, C. N.; Frank, C. W. Progress in the Development of Interpenetrating Polymer Network Hydrogels. *Polym. Adv. Technol.* **2008**, *19* (6), 647−657.
(11) Bin Ihsan, A.; Sun, T. L.; Kuroda, S.; Haque, M. A.; Kurokawa, T.; Nakajima, T.; Gong, J. P. A Phase Diagram of Neutral Polyampholyte - From Solution to Tough Hydrogel. *J. Mater. Chem. B* **2013**, *1* (36), 4555−4562.
(12) Nishi, K.; Shibayama, M. Probe-SAXS on Hydrogels under Elongation. *Soft Matter* **2016**, *12* (24), 5334−5339.
(13) Wiener, C. G.; Tyagi, M.; Liu, Y.; Weiss, R. A.; Vogt, B. D. Supramolecular Hydrophobic Aggregates in Hydrogels Partially Inhibit Ice Formation. *J. Phys. Chem. B* **2016**, *120* (24), 5543−5552.
(14) Tian, J.; Seery, T. A. P.; Ho, D. L.; Weiss, R. A. Physically cross-linked alkylacrylamide hydrogels: A SANS analysis of the microstructure. *Macromolecules* **2004**, *37* (26), 10001−10008.
(15) Hao, J. K.; Weiss, R. A. Tuning the Viscoelastic Behavior of Hybrid Hydrogels Composed of a Physical and a Chemical Network by the Addition of an Organic Solvent. *Macromolecules* **2016**, *49* (17), 6687−6693.
(16) Lu, J.; Bates, F. S.; Lodge, T. P. Remarkable Effect of Molecular Architecture on Chain Exchange in Triblock Copolymer Micelles. *Macromolecules* **2015**, *48* (8), 2667−2676.
(17) Peters, A. J.; Lodge, T. P. Comparison of Gel Relaxation Times and End-Block Pullout Times in ABA Triblock Copolymer Networks. *Macromolecules* **2016**, *49* (19), 7340−7349.
(18) Bae, S. S.; Chakrabarty, K.; Seery, T. A. P.; Weiss, R. A. Thermoprocessible Hydrogels. I. Synthesis and Properties of Polyacrylamides with Perfluoroalkyl Side Chains. *J. Macromol. Sci., Part A: Pure Appl.Chem.* **1999**, *36* (7−8), 931−948.
(19) Xie, X. Y.; HogenEsch, T. E. Copolymers of N,N-Dimethylacrylamide and 2-(N-Ethylperfluorooctanesulfonamido)Ethyl Acrylate in Aqueous Media and in Bulk. Synthesis and Properties. *Macromolecules* **1996**, *29* (5), 1734−1745.
(20) Stafford, C. M.; Guo, S.; Harrison, C.; Chiang, M. Y. M. Combinatorial and High-Throughput Measurements of the Modulus of Thin Polymer Films. *Rev. Sci. Instrum.* **2005**, *76* (6), 062207.
(21) Glinka, C. J.; Barker, J. G.; Hammouda, B.; Krueger, S.; Moyer, J. J.; Orts, W. J. The 30 m Small-Angle Neutron Scattering Instruments at the National Institute of Standards and Technology. *J. Appl. Crystallogr.* **1998**, *31*, 430−445.
(22) Kline, S. R. Reduction and Analysis of SANS and USANS Data using IGOR Pro. *J. Appl. Crystallogr.* **2006**, *39*, 895−900.
(23) Hammouda, B. *SANS Toolbox* **2010**, 692.
(24) Hirai, Y.; Terashima, T.; Takenaka, M.; Sawamoto, M. Precision Self-Assembly of Amphiphilic Random Copolymers into Uniform and Self-Sorting Nanocompartments in Water. *Macromolecules* **2016**, *49* (14), 5084−5091.
(25) Wignall, G. D.; Melnichenko, Y. B. Recent Applications of Small-Angle Neutron Scattering in Strongly Interacting Soft Condensed Matter. *Rep. Prog. Phys.* **2005**, *68* (8), 1761−1810.
(26) Wu, B.; Li, X.; Do, C.; Kim, T. H.; Shew, C. Y.; Liu, Y.; Yang, J.; Hong, K. L.; Porcar, L.; Chen, C. Y.; Liu, E. L.; Smith, G. S.; Herwig, K. W.; Chen, W. R. Spatial Distribution of Intra-Molecular Water and Polymeric Components in Polyelectrolyte Dendrimers Revealed by Small Angle Scattering Investigations. *J. Chem. Phys.* **2011**, *135* (14), 144903.
(27) Hao, J. K.; Weiss, R. A. Viscoelastic and Mechanical Behavior of Hydrophobically Modified Hydrogels. *Macromolecules* **2011**, *44* (23), 9390−9398.
(28) Nystrom, B.; Walderhaug, H. Dynamic Viscoelasticity of an Aqueous System of a Poly(ethylene oxide)-Poly(propylene oxide)-Poly(ethylene oxide) Triblock Copolymer during Gelation. *J. Phys. Chem.* **1996**, *100* (13), 5433−5439.
(29) Schiessel, H.; Metzler, R.; Blumen, A.; Nonnenmacher, T. F. Generalized Viscoelastic Models: Their Fractional Equations with Solutions. *J. Phys. A: Math. Gen.* **1995**, *28* (23), 6567−6584.
(30) Shibayama, M.; Karino, T.; Miyazaki, S.; Okabe, S.; Takehisa, T.; Haraguchi, K. Small-Angle Neutron Scattering Study on Uniaxially Stretched Poly(N-isopropylacrylamide)-Clay Nanocomposite Gels. *Macromolecules* **2005**, *38* (26), 10772−10781.
(31) Shibayama, M.; Kawakubo, K.; Ikkai, F.; Imai, M. Small-Angle Neutron Scattering Study on Charged Gels in Deformed State. *Macromolecules* **1998**, *31* (8), 2586−2592.
(32) Mendes, E.; Schosseler, F.; Isel, F.; Boue, F.; Bastide, J.; Candau, S. J. A SANS Study of Uniaxially Elongated Polyelectrolyte Gels. *Europhys. Lett.* **1995**, *32* (3), 273−278.
(33) Mendes, E.; Oeser, R.; Hayes, C.; Boue, F.; Bastide, J. Small-Angle Neutron Scattering Study of Swollen Elongated Gels: Butterfly Patterns. *Macromolecules* **1996**, *29* (17), 5574−5584.
(34) Oka, Y. I.; Sakohara, S.; Gotoh, T.; Iizawa, T.; Okamoto, K.; Doi, H. Measurements of Mechanical Properties on a Swollen Hydrogel by a Tension Test Method. *Polym. J.* **2004**, *36* (1), 59−63.

DOI: 10.1021/acs.macromol.6b02680
Macromolecules 2017, 50, 1672−1680